SYNTHETIC BIOLOGY

Photocatalyst-mineralized biofilms as living bio-abiotic interfaces for single enzyme to whole-cell photocatalytic applications

Xinyu Wang[1,2]†, Jicong Zhang[3]†, Ke Li[4], Bolin An[1,2], Yanyi Wang[1,2], Chao Zhong[1,2,3]*

There is an increasing trend of combining living cells with inorganic semiconductors to construct semi-artificial photosynthesis systems. Creating a robust and benign bio-abiotic interface is key to the success of such solar-to-chemical conversions but often faces a variety of challenges, including biocompatibility and the susceptibility of cell membrane to high-energy damage arising from direct interfacial contact. Here, we report living mineralized biofilms as an ultrastable and biocompatible bio-abiotic interface to implement single enzyme to whole-cell photocatalytic applications. These photocatalyst-mineralized biofilms exhibited efficient photoelectrical responses and were further exploited for diverse photocatalytic reaction systems including a whole-cell photocatalytic CO_2 reduction system enabled by the same biofilm-producing strain. Segregated from the extracellularly mineralized semiconductors, the bacteria remained alive even after 5 cycles of photocatalytic NADH regeneration reactions, and the biofilms could be easily regenerated. Our work thus demonstrates the construction of biocompatible interfaces using biofilm matrices and establishes proof of concept for future sustainable photocatalytic applications.

INTRODUCTION

Living biological material systems, in contrast with their nonliving counterparts, have an inimitable combination of features including environmental adaption, self-propagation, responsiveness to environmental stimuli, and self-repair ability (*1*–*4*). Inorganic systems, particularly inorganic nanomaterials such as semiconducting nanoparticles (NPs), have their own unique properties such as high surface-to-volume ratios, broad-range light-harvesting ability, and extremely efficient photoelectrochemical properties (*5*–*7*). Thus, the idea of combining biological and inorganic nanomaterial systems has attracted much attention, with researchers in multiple areas exploring potentially vast application opportunities in areas including catalysis (*8*), electronics (*9*), precision drug delivery (*10*), diagnostics (*11*), and disease treatment (*12*). In particular, the combination of living microbes with inorganic semiconductors has recently become a research hotspot in the nascent materials research field known as "semi-artificial photosynthesis" (*13*, *14*). In semi-artificial photosynthesis systems, the design of biocompatible interfaces to hybridize microbial cells and inorganic semiconductors is viewed as the key to achieve high-efficiency solar-driven fuel (such as H_2 or liquid alcohol) (*15*, *16*) or chemical production (such as complex metabolite shikimic acid) (*17*).

Several strategies have been previously reported for the integration of microbial cells with semiconducting NPs for photoinduced biocatalytic applications (*13*). Through CdS NP precipitation on the cell surface of the bacterium *Moorella thermoacetica*, photoinduced CO_2 fixation to acetic acid was achieved using photogenerated electrons as the reducing power (*18*). During the reaction procedure, the oxidative holes produced by CdS upon light irradiation caused cell damage and even complete cell rupture at higher light intensities. An alternative method, the "nanobiohybrid organism" was developed on the basis of the intracellular uptake of quantum dots (including CdS, CdSe, and InP QDs) into bacteria (including *Azotobacter vinelandii* and *Cupriavidus necator*) for photoinduced conversion of CO_2, N_2, and H_2O into renewable biochemicals (such as butanediol and poly-β-hydroxybutyric acid) (*19*). Despite having impressive catalytic activities, these systems unfortunately lacked a sustainable bio-abiotic interface for continuous solar-to-chemical conversion, as intracellular QDs could also impair the cell viability originating from the toxicity of the ligands (such as cysteamine or 3-mercaptopropionic acid) modified on the surface of QDs (*19*) or the insertion of NPs into the cell membrane (*20*). Thus, despite important progress, creation of ideal interfaces between cells and nanomaterials, which had both interfacial stability and minimum cell damage, was still an unresolved challenge due to functional differences between biological and inorganic nanosystems (*21*, *22*).

Biofilms are natural consortia of microbial cells embedded in their secreted extracellular matrix, composed of amyloid fibers exhibiting superior resilience to external environmental stresses (*23*, *24*). Here, inspired by the vast application potential of bacterial biofilms as engineered living materials (*2*) and biocatalysts (*24*), we developed an in situ mineralization strategy for the construction of photocatalyst-mineralized biofilms and harvested such mineralized biofilms as living bio-abiotic interfaces to implement diverse photocatalytic applications. Specifically, we first fused A7 peptides, containing two cysteines having strong affinity toward transition metal ions, to the C terminus of the *Escherichia coli* curli major subunit CsgA protein to construct functional $CsgA_{A7}$ nanofibers, which site-specifically promoted the in situ extracellular mineralization of CdS NPs. Then, we used functional $Tc_{Receiver}/CsgA_{A7}$ biofilms to generate photocatalyst-mineralized biofilms through in situ mineralization of CdS NPs on *E. coli* biofilm nanofibers, thereby retaining

[1]CAS Key Laboratory of Quantitative Engineering Biology, Shenzhen Institute of Synthetic Biology, Shenzhen Institute of Advanced Technology, Chinese Academy of Sciences, Shenzhen, China. [2]Center for Materials Synthetic Biology, Shenzhen Institute of Synthetic Biology, Shenzhen Institute of Advanced Technology, Chinese Academy of Sciences, Shenzhen 518055, China. [3]School of Physical Science and Technology, ShanghaiTech University, Shanghai 201210, China. [4]School of Food Science and Pharmaceutical Engineering, Nanjing Normal University, Nanjing 210000, China.
*Corresponding author. Email: chao.zhong@siat.ac.cn
†These authors contributed equally to this work.

the attractive photocatalytic potential of the hybrid catalyst while alleviating impairment through segregation of CdS NPs from bacterial cells (Fig. 1). The CdS NPs within photocatalyst-mineralized biofilms generated electrons upon light irradiation, and the electrons were used and transferred to the redox centers of catalytic enzymes via electron mediators [such as methyl viologen (MV) or nicotinamide adenine dinucleotide (NAD)]. Last, we successfully achieved single enzyme to whole-cell photocatalytic applications including photocatalytic trimethylpyruvic acid (TMP) reduction using purified leucine dehydrogenase (LDH) enzyme (Fig. 1A) and photocatalytic CO_2 reduction using a single whole cell coexpressing extracellular $CsgA_{A7}$ fibers and intracellular formate dehydrogenase (FDH) (Fig. 1B). In particular, the cells remained alive even after 5 cycles of photocatalytic NADH (reduced form of NAD^+) regeneration reactions. The proof-of-concept demonstration of cyclable photocatalytic applications suggested that the biofilms can serve as excellent platforms for the construction of biocompatible bio-abiotic interfaces for sustainable production of chemicals and stocks. Our constructed photocatalyst-mineralized biofilms exhibited alleviated injuries through segregation and higher catalytic efficiency through more active site exposure. The design expands the frontier of semi-artificial photosynthesis and has the potential to drive further research that can solve future energy and environmental issues.

RESULTS

Photocatalyst-mineralized biofilms produced by in situ mineralization of CdS NPs on biofilm nanofibers

We adopted a modular genetic design strategy (*25*) to generate functional $Tc_{Receiver}/CsgA_{A7}$ biofilms expressing recombinant $CsgA_{A7}$ nanofibers under the control of a tetracycline (Tc)–induced promoter (Fig. 2A and fig. S1). We first verified the extracellular production of functional $Tc_{Receiver}/CsgA_{A7}$ biofilms. Transmission electron microscope (TEM) analysis showed that recombinant functional curli nanofibers were expressed upon Tc induction in M63 culture for 2 days (Fig. 2A and fig. S2), and selected-area electron diffraction (SAED) analysis indicated that the curli nanofibers did not form any obvious crystalline structures (Fig. 2A, bottom left). Congo red (CR) binding assays and crystal violet (CV) staining supported the amyloid nature of the secreted nanofibers (fig. S3). We next added precursors $CdCl_2$ and excess Na_2S to the culture medium to induce the formation of photocatalyst-mineralized biofilms. The in situ mineralization of CdS NPs on recombinant $CsgA_{A7}$ nanofibers was designed to synchronize with biofilm formation, and TEM revealed that agglomerates had formed on the curli fibers after 2 days of cultivation (Fig. 2B). The resulting photocatalyst-mineralized biofilms exhibit a clear diffraction ring assigned to the (100) plane from the SAED results (Fig. 2B, bottom left), apparently corresponding to the 0.35-nm space lattice of CdS structures revealed by high-resolution TEM (HRTEM) (Fig. 2C, bottom left).

We used high-angle annular dark-field scanning TEM (HAADF-STEM) and energy-dispersive x-ray spectroscopy (EDS) mapping to further characterize the photocatalyst-mineralized biofilms (Fig. 2, C and D, and fig. S4), and the presence of both Cd and S confirmed successful in situ mineralization of the desired CdS NPs on the $CsgA_{A7}$ nanofibers. X-ray photoelectron spectroscopy (XPS), a technique that can measure the elemental composition of a material, confirmed the presence of Cd (405 and 411.7 eV) and S (163.3 eV) in the CdS-mineralized biofilms (Fig. 2, E and F, and fig. S5), supporting our initial EDS mapping results. The signals for O, N, and P came from biological components within the CdS-mineralized biofilms.

We further used inductively coupled plasma optical emission spectrometry (ICP-OES) to monitor the free Cd^{2+} ion concentration at different cultivation intervals during the mineralization process

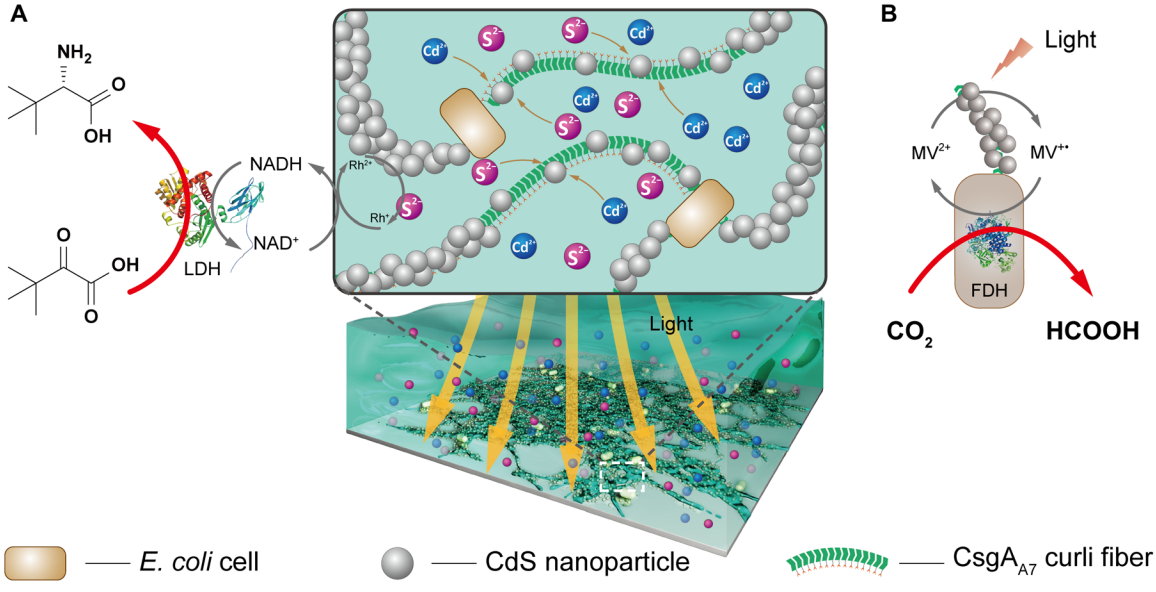

Fig. 1. Schematic of living photocatalyst-mineralized biofilms explored for single enzyme to whole-cell photocatalysis. The A7 peptides within the biofilms are functional peptides specifically displayed on the $CsgA_{A7}$ nanofibers that can be mineralized via in situ formation of CdS NPs generating photocatalyst-mineralized biofilms. The mineralized biofilms harbor the CdS NPs that can produce electrons upon light irradiation; the electrons are then harnessed and transferred to the catalytic centers of redox enzymes through electron mediators (MV or NAD) for various photocatalytic applications including reduction of TMP into L-tert-leucine coupling with purified LDH (**A**) and CO_2 reduction coupling with a single cell coexpressing $CsgA_{A7}$ fibers and FDH (**B**).

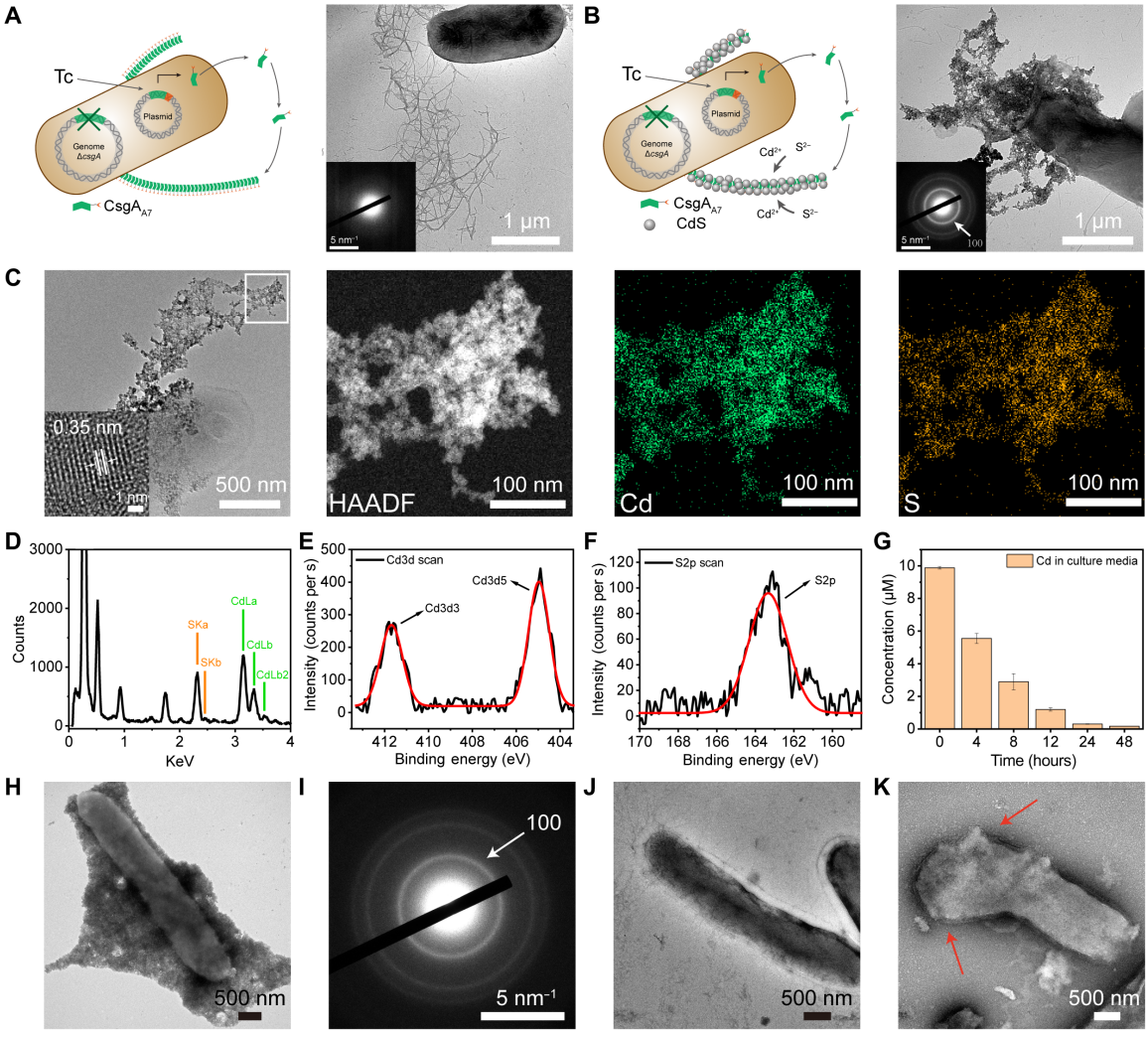

Fig. 2. Characterization of the functional biofilms mineralized with CdS NPs. (**A**) Schematic of the formation process for $Tc_{Receiver}/CsgA_{A7}$ biofilms and their TEM and SAED images. (**B**) Schematic of the in situ mineralization process on biofilm curli nanofibers and TEM and SAED (inset) images of the CdS-mineralized biofilms. The mineralized biofilms exhibited a clear diffraction ring, whereas the $Tc_{Receiver}/CsgA_{A7}$ biofilms did not. The (100) corresponds to the space lattice of 0.35 nm for the CdS NPs in (C). (**C** and **D**) HRTEM, HAADF-STEM, and EDS mapping images of the nanofiber/CdS composites in the mineralized biofilms. The green represents Cd atoms, and the orange represents S atoms. (**E** and **F**) XPS spectra of CdS-mineralized biofilms, which confirmed the presence of Cd and S atoms, in accordance with the EDS mapping results. The red curves were fitted curves to accurately determine the peak value position. (**G**) Inductively coupled plasma optical emission spectrometry (ICP-OES) results for measurement of free Cd^{2+} ion concentrations in the supernatant during the process of in situ mineralization of CdS NPs on biofilms in M63 cultivation medium over a 2-day period. (**H** and **I**) TEM (H) and SAED (I) images for the $Tc_{Receiver}/ompA_{A7}$ sample mineralized with CdS NPs. (**J** and **K**) TEM images for the CdS-mineralized biofilms (J) and CdS-mineralized $Tc_{Receiver}/ompA_{A7}$ cells (K) after irradiation for 24 hours by an artificial blue light. The red arrows pointed to the damaged cell parts.

(Fig. 2G). We set the starting Cd^{2+} concentration as 9.88 ± 0.078 μM in the culture medium. There was a marked decrease in Cd^{2+} concentration in the supernatant of the culture medium with the increasing cultivation time, with Cd^{2+} in the culture medium with 3.05% (0.30 ± 0.015 μM) and 1.71% (0.17 ± 0.023 μM) remaining after 24 and 48 hours of cultivation, respectively. These observations support that the in situ mineralization of CdS NPs on recombinant $CsgA_{A7}$ nanofibers was synchronized with the biofilm formation. The CdS NPs did not cause detectable damage to the biofilms, as integral cell structures were evident in the TEM images (Fig. 2B and fig. S6). Furthermore, we recultivated both photocatalyst-mineralized biofilms and nonmineralized control $Tc_{Receiver}/CsgA_{A7}$ biofilms. Both mineralized and nonmineralized samples displayed nearly equal growth curves, further indicating that the formation of CdS NPs did not cause obvious toxicity to the cells (fig. S7).

We next constructed another strain ($Tc_{Receiver}/ompA_{A7}$) that could display A7 peptides on the cell membrane under the induction of Tc and carried out the same in situ mineralization experiments to determine whether mineralized structures in biofilms would substantially minimize the potential high-energy damage caused to cells under light illumination. We selected artificial blue light arrays with emissions at 455 to 460 nm to test the protective ability of biofilms on cells because mineralized CdS NPs had absorption below 515 nm in the blue light region (Fig. 3, A and B). TEM images showed that, after in situ mineralization, the cells were surrounded by mineralized NPs (Fig. 2H and figs. S8 and S9). The identity of the NPs was

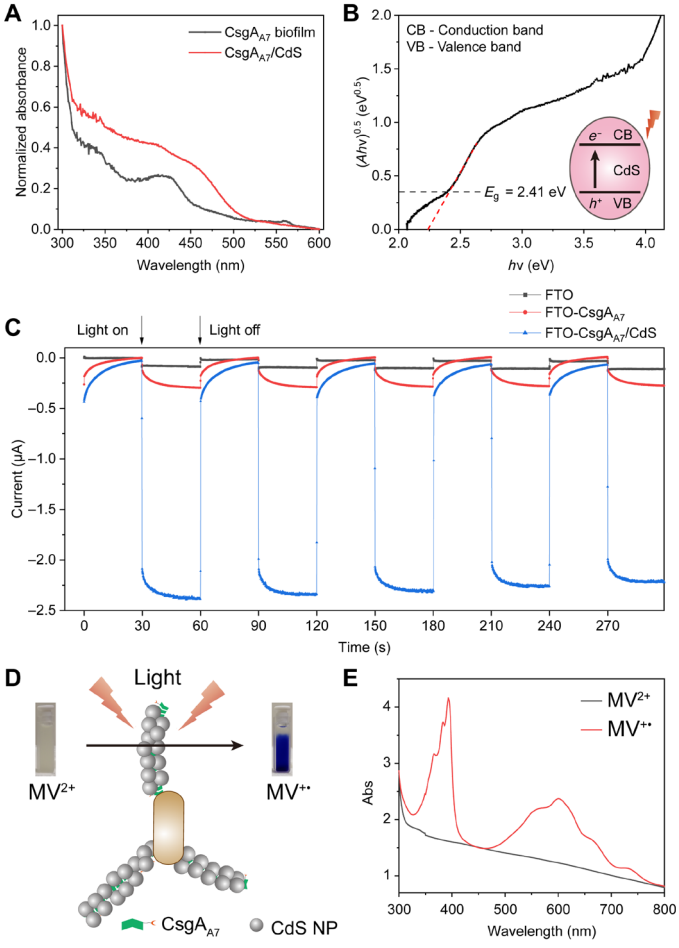

Fig. 3. Photoelectric properties of the photocatalyst-mineralized biofilms. (**A**) Ultraviolet-visible (UV-vis) spectra of the $Tc_{Receiver}/CsgA_{A7}$ biofilms and the photocatalyst-mineralized biofilms. (**B**) The bandgap of the CdS NPs formed within the photocatalyst-mineralized biofilms. *A* is the normalized absorption value, *h* is the Planck's constant (6.626×10^{-34} J·s), and *v* is the frequency. (**C**) Transient photocurrent curves measured through a three-electrode system, where FTO-conductive glass deposited with biofilm samples served as the working electrode and a platinum wire served as the counter electrode; there was also a Ag/AgCl reference electrode. The blue curve represents the photocurrent of the FTO glass (1 cm by 1 cm) deposited with photocatalyst-mineralized biofilms, upon illumination (light on) or shielding (light off) from a Xe lamp. The red and black curves represent the photocurrent of the FTO glass (1 cm by 1 cm) deposited with $Tc_{Receiver}/CsgA_{A7}$ biofilms or bare FTO glass, respectively. (**D**) Schematic of photocatalytic electron transfer to MV via the photocatalyst-mineralized biofilms. The 3-ml tris-HCl reaction solution was put into a cuvette containing 1 mM MV^{2+} (as the electron mediator), 1.5% TEOA (as the sacrificial agent), and the photocatalyst-mineralized biofilms. The reaction solution was irradiated for 12 hours, during which colorless MV^{2+} was converted to violet $MV^{+\bullet}$. (**E**) UV-vis spectra for MV^{2+} and its reduced form $MV^{+\bullet}$. In (A and C), "$CsgA_{A7}$" refers to $Tc_{Receiver}/CsgA_{A7}$ biofilms. "$CsgA_{A7}$/CdS" refers to photocatalyst-mineralized biofilms.

verified as CdS by the clear diffraction ring of the (100) plane (Fig. 2I). Both CdS-mineralized $Tc_{Receiver}/CsgA_{A7}$ biofilms and CdS-mineralized $Tc_{Receiver}/ompA_{A7}$ cells were collected and exposed to an artificial blue light for 24 hours, followed by streak plating experiment, TEM analysis, and live/dead staining. The biofilm samples had more living cells (survival rate of 86.8 ± 0.6%) indicated by the clear appearance of individual colonies on the plate, while $Tc_{Receiver}/ompA_{A7}$ cells had minimal colonies (survival rate of 48.6 ± 2.2%) germinated (fig. S10) in accordance with live/dead staining results (fig. S11). In addition, the cells in the biofilms were almost integral, while the surface-displayed bacterial cells were partially damaged or even fractured, as clearly shown by TEM images (Fig. 2, J and K, and fig. S12). Green (emissions at 520 to 525 nm) and red (620 to 625 nm) light imposed minor injuries to bacterial cells due to an inefficient energy supply for CdS activation to generate electron-hole pairs (figs. S13 and S14). These results indicated that a biocompatible bio-abiotic interface could be enabled by mineralized biofilms. Thus, we achieved in situ mineralization of CdS NPs on engineered curli fibers, allowing construction of a biocompatible living bio-inorganic interface for subsequent photocatalytic applications.

Photoelectric properties of the photocatalyst-mineralized biofilms

CdS NPs are nanoscale materials with potential for various catalysis applications (*7*). Therefore, we experimentally verified whether our CdS-mineralized biofilms would have excellent photoelectric properties. First, we characterized the CdS bandgap by recording ultraviolet and visible diffuse reflectance spectra (UV-vis DRS) using dried CdS-mineralized biofilms prepared through vacuum drying. The photocatalyst-mineralized biofilms had broader absorbance in the visible region compared with $Tc_{Receiver}/CsgA_{A7}$ biofilms (Fig. 3A). We then plotted the $(Ahν)^{0.5}$ (with *hν*) values and calculated the CdS NP bandgap on the basis of the inflection point for the processed curve (Fig. 3B): The bandgap of the CdS NPs presented in the photocatalyst-mineralized biofilms was determined to be 2.41 eV in correspondence to the absorption at 515 nm, similar to the value found in previous reports (*7*, *26*, *27*).

We next used both transient photocurrent and MV reduction tests to determine whether the photoinduced electrons from the CdS NPs within photocatalyst-mineralized biofilms could be transferred and harnessed for our desired applications. Biofilm samples were collected from 20 ml of M63 culture medium and resuspended in 1 ml of ddH_2O. An fluorine doped tin oxide (FTO)-conductive glass (1 cm by 1 cm) substrate was exposed to the sample solution containing different biofilms and was dried in an incubator at 37°C for 12 hours. We adopted a three-electrode system to record the photoinduced transient current, where the biofilm sample–coated FTO was used as the working electrode, a platinum wire as the counter electrode, and a Ag/AgCl electrode as the reference electrode; the system used 0.5 M Na_2SO_4 as the electrolyte solution, and the irradiation was from a Xe lamp (Fig. 3C and fig. S15). A transient current of 2.4 μA commenced upon illumination of the photocatalyst-mineralized biofilms: a value much larger than for the bare FTO glass (0.08 μA) or the $Tc_{Receiver}/CsgA_{A7}$ biofilm–coated FTO glass (0.3 μA). These results strongly support the photocurrent-induced transfer of electrons from the photocatalyst-mineralized biofilms to the electrode and indicate their potential for photocatalytic applications.

MV is a commonly used electron mediator agent in photocatalytic applications (*26*). Having detected photoinduced electron transference with electrodes, we next verified whether the electrons could be transferred to MV from the irradiated CdS NPs within the photocatalyst-mineralized biofilms. Our reaction solution was placed in a cuvette with 1.5% triethanolamine (TEOA) as the sacrificial agent. Upon light illumination, the CdS NPs generated electrons that transformed MV from the colorless MV^{2+} form into its violet $MV^{+\bullet}$ form (Fig. 3D). The UV-vis spectra clearly exhibited two peaks between 300 to 400 nm and 500 to 700 nm (Fig. 3E), confirming

$MV^{+\bullet}$ formation upon illumination. Note that MV alone was not sufficient to form MV radicals under irradiation of 365-nm UV light (fig. S16). These results collectively establish a proof of concept for the use of our photocatalyst-mineralized biofilms to achieve electron export upon light irradiation, supporting that our system works as designed and should be suitable for use in photocatalytic applications.

Photocatalytic reduction of TMP into L-tert-leucine using purified LDH enzyme

Having shown that our photocatalyst-mineralized biofilms can transfer electrons from the extracellular CdS NPs to an electron mediator compound, we next turned to explore bioproduction applications requiring reductants. Here, focusing on producing the coenzyme NADH to support reduction of TMP into L-tert-leucine, we replaced MV as the electron mediator with the Rh complex (fig. S17), which has been reported to efficiently generate biologically active NADH (*28*). Our reaction design combined the Rh complex with our photocatalyst-mineralized biofilms and included the addition of purified LDH enzyme (Fig. 4A). In this design, light irradiation should cause transfer of electrons from the CdS NPs within the photocatalyst-mineralized biofilms to drive the conversion of $[Cp^*Rh(bpy)H_2O]^{2+}$ (Rh^{2+}) to $[Cp^*Rh(bpy)H]^{+}$ (Rh^{+}), which can, in turn, reduce NAD^+ to form NADH; subsequently, the substrate TMP can be reduced to L-tert-leucine by LDH assisted by the coenzyme NADH.

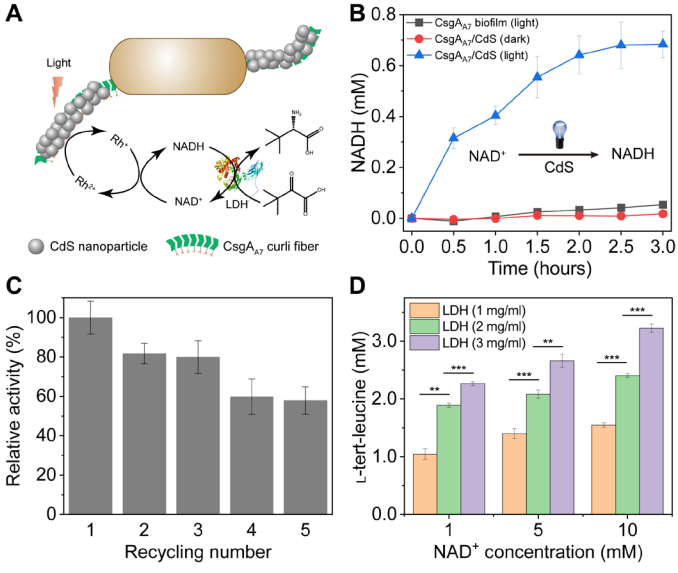

Fig. 4. Photocatalytic reduction of TMP into L-tert-leucine coupling with purified LDH enzyme. (**A**) Schematic of the TMP reduction process, where CdS NPs within the photocatalyst-mineralized biofilms absorb light and produce electrons. (**B**) NAD^+ reduction under different reaction systems using artificial blue light-emitting diode (LED) arrays as the light source. "$CsgA_{A7}$ biofilm (light)" refers to the reaction system using $Tc_{Receiver}/CsgA_{A7}$ biofilms; "$CsgA_{A7}$/CdS (dark)" refers to the reaction system without illumination. (**C**) Relative activity comparison for five consecutive reactions, for which the photocatalyst-mineralized biofilms were recycled for use each time after 3 hours of illumination. These 1-ml reaction solutions (in tris-HCl solution, pH 8.0) contained 1 mM NAD^+, 1.5% TEOA, 0.25 mM $[Cp^*Rh(bpy)H_2O]^{2+}$, and the recycled photocatalyst-mineralized biofilms (with pellets were originally collected from 20 ml of M63 culture medium and recovered via centrifugation and resuspension after each of the reactions). (**D**) Reduction of TMP to L-tert-leucine under different reaction systems using artificial blue LED arrays as the light source. The 1-ml tris-HCl reaction solution (pH 8.0) contained LDH (1, 2, or 3 mg/ml), 1.5% TEOA, NAD^+ (1, 5, or 10 mM), 0.25 mM $[Cp^*Rh(bpy)H_2O]^{2+}$, 10 mM TMP, 10 mM NH_4Cl, and photocatalyst-mineralized biofilms. Each experiment was repeated three times. Student's *t* test, $^{**}P < 0.01$, and $^{***}P < 0.001$.

We first assessed the generation of NADH in reactions combining the photocatalyst-mineralized biofilms, 1 mM NAD^+, 0.25 mM Rh^{2+}, and 1.5% of TEOA (the sacrificial agent) in 1 ml of tris-HCl solution upon illumination (fig. S18). NADH generation was monitored at 340 nm (figs. S19 and S20): We found that the NADH concentration reached a plateau at 0.68 mM within 3 hours, representing a final NAD^+ to NADH conversion efficiency of 68% (Fig. 4B). Only negligible NADH was detected under dark conditions or in the reaction system with the nonmineralized $Tc_{Receiver}/CsgA_{A7}$ biofilms (Fig. 4B). We further tested the recyclability of our photocatalyst-mineralized biofilms by centrifugation. For easy comparison, we defined the relative activity as the concentration ratios of each cycle to the first cycle. After 5 cycles of reaction, our functional biofilms retained nearly 60% of the initial activity (Fig. 4C and fig. S21). Notably, we found that CdS NPs were still anchored on the biofilms and that parts of the cells remained integral and alive compared with their pristine states revealed by TEM images, strain streak plating experiments, and live/dead staining experiments (survival rate of 47.2 ± 3.2% for the first cycle and 13.5 ± 4.2% for the fifth cycle) (figs. S22 to S24).

After detecting successful NADH generation, we tested a reaction system comprising LDH enzyme, TEOA, NAD^+, Rh^{2+}, the two cosubstrates (TMP and NH_4Cl), and the photocatalyst-mineralized biofilms in 1 ml of tris-HCl solution. The nuclear magnetic resonance (NMR) peak for the methyl group moved from 1.195 to 1.059 parts per million (ppm), supporting the production of L-tert-leucine from TMP (fig. S25). We found that concentrations of both NAD and LDH coaffected the production of L-tert-leucine (Fig. 4D and fig. S26). The highest output of 3.23 mM of L-tert-leucine was achieved with the 10 mM NAD^+ and LDH system (3 mg/ml). These experiments demonstrate the successful reduction of TMP to form L-tert-leucine and establish the capacity of our photocatalyst-mineralized biofilms for multicomponent redox bioproduction applications.

Photocatalytic CO_2 reduction

The use of biofilms for bioproduction and other industrial applications is desirable because it can support the use of whole cells (*24*), representing a highly scalable platform for achieving solar-driven chemicals. We explored whole-cell photocatalytic systems based on our photocatalyst-mineralized biofilms. Beyond the capacity for easy scale-up, another attractive aspect of whole cell–based systems is the ability to genetically engineer additional functionalities into a single strain. Therefore, we designed a single-strain system for an additional photocatalytic application: reduction of CO_2 to HCOOH using MV as the mediator (Fig. 5A and fig. S27). We constructed the engineered *E. coli* $Tc_{Receiver}/CsgA_{A7}$-FDH system, which had two benefits. First, the expressed biofilms were used as nucleator for CdS mineralization, which could expose more active sites for catalysis compared with the system established with exogenously added carboxyl-capped CdS NPs. Second, the expression of intracellular FDH enzymes could occur simultaneously to simplify the system setup and fulfill whole-cell catalysis with the same biofilm-producing strain, thus substantially outperforming a two-strain catalytic system based on our previous reports (*29*).

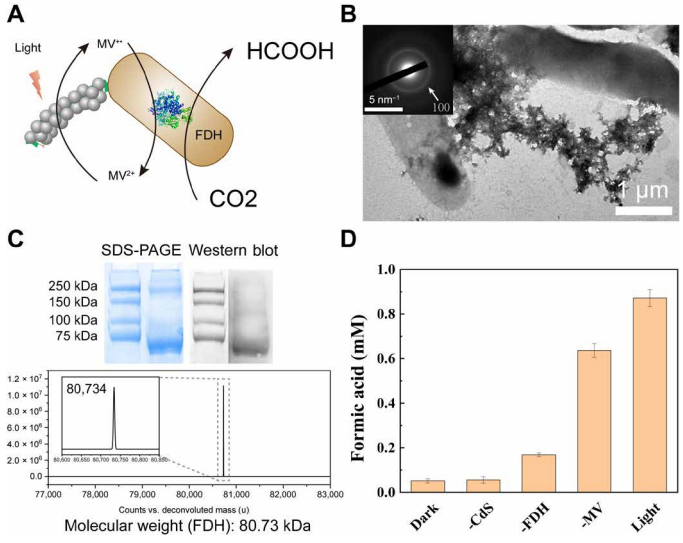

Fig. 5. Whole cell–enabled photocatalytic CO_2 reduction. (**A**) Schematic of a photocatalytic CO_2 reduction system based on a single strain coexpressing $CsgA_{A7}$ nanofibers for CdS mineralization and FDH enzymes for CO_2 reduction. (**B**) TEM image of the photocatalyst-mineralized biofilms through in situ mineralization on $Tc_{Receiver}$/$CsgA_{A7}$-FDH biofilms. (**C**) SDS-PAGE image, Western blot image, and LC-MS spectrum for the purified FDH enzymes from $Tc_{Receiver}$/$CsgA_{A7}$-FDH biofilms. (**D**) Photocatalytic CO_2 reduction under different reaction conditions. "Light" refers to a reaction system comprising 5 mM MV, 10 mM ascorbic acid, 100 mM $NaHCO_3$, and the photocatalyst-mineralized biofilms in PBS solution (pH 7.4) under normal illumination condition. "Dark" refers to the same reaction system but lacking illumination. "–FDH" refers to an illuminated reaction system without expression of FDH enzymes. "–CdS" refers to an illuminated reaction system with $Tc_{Receiver}$/$CsgA_{A7}$-FDH biofilms that were not mineralized with CdS NPs. "–MV" refers to an illuminated reaction system without MV.

Here, the $Tc_{Receiver}$/$CsgA_{A7}$-FDH biofilm–producing strain was engineered to coexpress $CsgA_{A7}$ nanofibers and FDH enzymes under the control of the Tc-induced promoter and the constitutive J23108 promoter, respectively (fig. S28) (*30*). TEM and SAED analysis confirmed that this strain produced $CsgA_{A7}$ nanofibers that could be in situ mineralized with CdS NPs (Fig. 5B and fig. S29). Furthermore, after collecting and lysing the biofilms, SDS–polyacrylamide gel electrophoresis (SDS-PAGE), Western blot, and liquid chromatography–mass spectrometry (LC-MS) results confirmed that the cells expressed the engineered FDH enzymes with the anticipated molecular weight of 80.73 kDa (Fig. 5C and fig. S30) in accordance with previous report (*31*). The bands of FDH was absent in the supernatant after biofilm collection, which implied no secretion of FDH enzymes (fig. S31A). We also constructed $Tc_{Receiver}$/$CsgA_{A7}$-enhanced green fluorescent protein (mEGFP)-FDH cells to express mEGFP-FDH enzymes. The green fluorescence appeared clearly within the bacterial cells, which further supported the intracellular expression of FDH proteins in *E. coli* (fig. S31B). These results demonstrated the successful coproduction of $CsgA_{A7}$ curli nanofibers and FDH enzymes in our constructed single whole cell.

We conducted reactions using the reaction system containing MV as the electron mediators, ascorbic acid as the sacrificial agent, $NaHCO_3$ as the CO_2 source, and the photocatalyst-mineralized biofilms in phosphate-buffered saline (PBS) solution. The presence of the characteristic peak for formic acid in the ^1H NMR spectrum at 8.44 ppm (fig. S32) (*32*) supported the quantification of the formic acid concentration from our system. The production of formic acid reached 0.84 mM within 8 hours under illumination with the Xe lamp (Fig. 5D and fig. S32), corresponding to the apparent quantum yield of ca. 0.13% in 8 hours, which was close to the efficiency of natural plants (*33*). There was negligible amount of formic acid production in the control reaction systems with nonmineralized $Tc_{Receiver}$/$CsgA_{A7}$-FDH biofilms, without illumination or without FDH expression. Furthermore, there was a 36% increase compared with the control group without MV addition, implying that uncharacterized electron transfer routes may occur between semiconductors and bacterial cells. We also performed photocatalytic CO_2 reduction combining carboxyl-capped CdS NPs with bacteria cells expressing FDH enzymes (fig. S33). The mineralized system had a 2.5-fold enhancement in formic acid production over that of the mixed system, where the higher efficiency probably originated from increased active site exposure due to low ligand occupation.

Compared with individual cells, bacterial biofilms are featured with large specific surface area, enhanced environmental tolerance under harsh conditions, and ease of functional modification through genetic engineering. The whole-cell photocatalysis coordinated single strain illustrates both conceptual and practical advances compared with the previous two-strain system, showing the potential for exploiting biofilm-enabled semi-artificial photosynthesis systems for sustainable solar-to-chemical conversions. The more precise tunability of semiconductors and exquisite gene regulations enabled by our benign biofilm-semiconductor systems would allow scalable value-added chemical production in the future.

DISCUSSION

The design of biocompatible interfaces between microbes and semiconductors holds great promise for diverse applications, especially for sustainable production of chemicals through technologies from the emerging area of semi-artificial photosynthesis (*14*). Seeking to alleviate the possible damage that can occur at the cell-inorganic interfaces in photocatalytic systems (*18*, *20*), we here produced living bio-abiotic interfaces where *E. coli* biofilms engineered with $CsgA_{A7}$ curli nanofibers as scaffolds for mineralization with CdS NPs were used to construct bio-abiotic interfaces that spatially segregate the mineralized CdS NP component from the bacterial cells. After mineralization, these NPs retained their useful photoelectric properties and functioned as efficient semiconductors. We showed that our photocatalyst-mineralized biofilms can achieve photocatalyzed transfer of electrons to diverse electron mediator compounds. We then exploited these photoinduced electrons for diverse photocatalytic applications, including redox-based synthesis of L-tert-leucine with an exogenously applied enzyme, and reduction of CO_2 to generate formic acid using a single engineered bacterial strain producing both the $CsgA_{A7}$ nanofibers and the FDH enzyme.

Previous attempts for the design of bio-abiotic interfaces include anchoring QDs on *E. coli* biofilms for photocatalytic H_2 production (*29*) and growing *Sporomusa ovata* biofilms on the silicon nanowire array electrode for acetate production coupling with a photovoltaic device (*34*). The preparation of QDs and silicon nanowire arrays necessarily involves the use of toxic reagents and harsh reaction conditions, while the coupling of the biofilm chassis with biomediated synthesis of nanomaterials, introduced in the current work, represents an important advantage over previous approaches owing to the simple, mild, and environmentally friendly reaction conditions

(*35*, *36*). Furthermore, our initial demonstration clearly illustrates the utility of this approach for enabling seamless integration of inorganic and biological materials while protecting delicate cells from damage by high–energy state semiconductor for photocatalytic applications.

Given that diverse types of amyloid nanofibers are widespread in nature, for example, in the Gram-positive *Bacillus subtilis (37)* or the facultative *Shewanella oneidensis* famous for its electron conductive capacity (*38*), the design principles demonstrated in the present study could be extended to other biofilm systems. In particular, the capacity to engineer the genomes of the various host strains should support the transfer of additional metabolic modules for applications in additional areas of semi-artificial photosynthesis or other pathways that require extensive local generation of reductants (e.g., NADH and NAD phosphate).

MATERIALS AND METHODS

Chemicals used in this study

Luria-Bertani (LB) medium (MdBio), chloramphenicol (Aladdin), M63 medium (AMRESCO), $MgSO_4$ [analytical reagent (AR); Sinopharm], glucose (ABCONE), Tc (Energy Chemical), K_2WO_4 (Aladdin), Na_2S (Macklin), $CdCl_2$ (Aladdin), 3-mercaptopropionic acid (Aladdin), glycerol (Aladdin), isopropyl-β-D-thiogalactoside (IPTG; Aladdin), carbenicillin (Macklin), tris-HCl (Promega), lysozyme (BBI), Na_2SO_4 (AR; Sinopharm), $[Rh(Cp^*)Cl_2]_2$ (Tansoole), methanol (Adamas), 2,2′-bipyridyl (Sinocompound), diethyl ether (AR; Sinopharm), triethanolamine (TEOA; Aladdin), NAD^+ (Solarbio), TMP (Adamas), NH_4Cl (AR; Sinopharm) MV (Aladdin), ascorbic acid (AR; Sinopharm), $NaHCO_3$ (Aladdin), CR (Aladdin), CV (BBI), PBS (ABCONE), uranyl acetate (Zhongjingkeyi Technology), $BaSO_4$ powder (Aladdin), D_2O (J&K), and 4,4-dimethyl-4-silapentane-1-sulfonic acid (DSS; Aladdin).

Plasmid and strain construction

Construction of Tc-inducible plasmid (pZA-CmR-rr12-pL(tetO)-CG-csgAA7)

The pZA-CmR-rr12-pL(tetO)-CG plasmid was used as a starting point (*39*). Recombinant gene combining CsgA and its biological secretion signal sequence with appended C-terminal A7 tag was obtained by standard PCR (polymerase chain reaction). The gene was then cloned into the pZA-CmR-rr12-pL(tetO)-CG vector through One-step Isothermal Gibson Assembly to produce the recombinant plasmid pZA-CmR-rr12-pL(tetO)-CG-*csgA*$_{A7}$. Plasmid sequences were confirmed by restriction digest and sequenced by Genewiz. The gene and protein sequences were included in tables S1 and S2.

Construction of recombinant plasmid surface displaying A7 peptides (pZA-CmR-rr12-pL(tetO)-ompAA7)

The pZA-CmR-rr12-pL(tetO) plasmid was used as the starting point. The *ompA*$_{A7}$ gene was obtained through standard PCR. The gene was cloned into the pZA-CmR-rr12-pL(tetO) vector through One-step Isothermal Gibson Assembly to produce the recombinant plasmid pZA-CmR-rr12-pL(tetO)-*ompA*$_{A7}$. Plasmid sequences were confirmed by restriction digest and sequenced by Genewiz. The gene and protein sequences were included in tables S1 and S2.

Construction of plasmid expressing LDH (pET22b-LDH)

The LDH gene was synthesized and then inserted into pET22b to form the recombinant plasmid pET22b-*LDH*. The obtained plasmid was sequenced by Genewiz. The gene and protein sequences were in included tables S1 and S2.

Construction of recombinant plasmid ptet-csgAA7-FDH expressing CsgAA7 and FDH

The ptet-*CsgA*$_{A7}$ plasmid was used as the starting point and linearized through standard PCR reaction. The FDH fragment with a constitutive expression promoter J23108 was obtained through standard PCR reaction. Last, the recombinant plasmid ptet-*CsgA*$_{A7}$-*FDH* was constructed by fusion of linearized ptet-*csgA*$_{A7}$ and FDH fragment through Gibson assembly. The obtained plasmid was sequenced by Genewiz. The gene and protein sequences were included in tables S1 and S2.

Construction of recombinant plasmid ptet-csgAA7-mEGFP-FDH expressing CsgAA7 and mEGFP-FDH

The ptet-*csgA*$_{A7}$-*FDH* plasmid was used as the starting point and linearized through standard PCR reaction. The mEGFP fragments were obtained through standard PCR reaction. Then, the recombinant plasmid ptet-*csgA*$_{A7}$-*mEGFP-FDH* was constructed by fusion of linearized ptet-*csgA*$_{A7}$-*FDH* and mEGFP fragment through One-step Isothermal Gibson Assembly. The obtained plasmid was sequenced by Genewiz. The gene and protein sequences were included in tables S1 and S2.

Strain construction

Cell strains used in this study were created by transforming the constructed plasmids into corresponding competent cells. MG 1655 *PRO* Δ*csgA ompR234* cells harboring a pZA-CmR-rr12-pL(tetO)-*csgA*$_{A7}$ plasmid were referred as *E. coli* $Tc_{Receiver}$/$CsgA_{A7}$ cells in this study. MG 1655 *PRO* Δ*csgA ompR234* cells harboring a ptet-*csgA*$_{A7}$-*FDH* plasmid were referred as *E. coli* $Tc_{Receiver}$/$CsgA_{A7}$-FDH cells in this study. MG 1655 *PRO* Δ*csgA ompR234* cells harboring a ptet-*csgA*$_{A7}$-*mEGFP-FDH* plasmid were referred as *E. coli* $Tc_{Receiver}$/$CsgA_{A7}$-mEGFP-FDH cells in this study. MG 1655 *PRO* Δ*csgA ompR234* cells harboring a pZA-CmR-rr12-pL(tetO)-*ompA*$_{A7}$ plasmid were referred as *E. coli* $Tc_{Receiver}$/$ompA_{A7}$ cells in this study. BL21(DE3)/LDH represents *E. coli* BL21(DE3) cell harboring the pET-22b-LDH plasmid in this study.

Biofilm cultivation

Seed cultures ($Tc_{Receiver}$/$CsgA_{A7}$ or $Tc_{Receiver}$/$CsgA_{A7}$-FDH) were inoculated from frozen glycerol stocks and grown in LB medium using chloramphenicol antibiotics (34 μg/ml). The cultures were grown for 12 hours at 37°C in 14-ml culture tubes (Falcon) with the 220 rpm shake speed. Cells were centrifuged and resuspended in the same volume of M63 medium, supplemented with 1 mM $MgSO_4$, 0.2% (w/v) glucose, chloramphenicol (34 μg/ml), and Tc (250 ng/ml) as inducer (hereafter referred to glucose-supplemented M63). The resuspended cells were used as seeds and added to M63 culture medium at a volume ratio of 1:100. The biofilm growth was performed by putting the experimental cultures into an incubator (Shanghai Yiheng) and cultivating for 48 hours at 30°C without shaking. The control experiments were carried out using glucose-supplemented M63 culture medium without Tc.

When using $Tc_{Receiver}$/$CsgA_{A7}$-FDH cells, the M63 culture was supplemented with extra 10 μM K_2WO_4. This system would allow the coproduction of $CsgA_{A7}$ nanofibers and FDH enzymes in the cultivation process.

Production of photocatalyst-mineralized biofilms

Seed cultures ($Tc_{Receiver}$/$CsgA_{A7}$, $Tc_{Receiver}$/$CsgA_{A7}$-FDH, and $Tc_{Receiver}$/$ompA_{A7}$) were inoculated from frozen glycerol stocks and grown in LB medium using chloramphenicol antibiotics (34 μg/ml). The cultures

were grown for 12 hours at 37°C in 14-ml culture tubes (Falcon) with the shake speed of 220 rpm. Cells were centrifuged and resuspended in the same volume of glucose supplementary M63 culture medium. The resuspended cells were used as seeds and added to glucose supplementary M63 culture medium at a volume ratio of 1:100. A total of 100 μl of Na_2S (0.1 M) and 100 μl of $CdCl_2$ (0.01 M) were added to a petri dish (90 mm; BBI) with 20 ml of glucose-supplemented M63 culture medium. The petri dish was put into the incubator (Shanghai Yiheng) and cultivated at 30°C without shaking. The samples cultivated for 2 days were scraped and collected through centrifugation. The collected photocatalyst-mineralized biofilms were directly used for the subsequent experiment.

When using $Tc_{Receiver}$/$CsgA_{A7}$-FDH cells, the culture was supplemented with extra 10 μM K_2WO_4. This system would allow the coproduction of $CsgA_{A7}$ nanofibers and FDH enzymes in the cultivation process.

When preparing for the ICP-OES measurement, 20 μl of Na_2S (0.1 M) and 20 μl of $CdCl_2$ (0.01 M) were added to 20 ml of M63 culture medium for the synthesis of CdS NPs. The concentration of Cd^{2+} in the supernatant was measured at different time interval using ICP-OES iCAP 7400 (Thermo Fisher Scientific).

LDH expression and purification

LDH expression

Seed cultures [BL21(DE3)/LDH] were inoculated from frozen glycerol stocks and grown in LB medium with carbenicillin (50 μg/ml). The cultures were grown for 12 hours at 37°C in 250-ml flasks, with a constant shake speed of 220 rpm. The seed cells were added to LB medium supplemented with carbenicillin (50 μg/ml) at a volume ratio of 1:50. The strains were grown for 3 hours at 37°C with a constant shaking speed at 220 rpm. The LDH expression was induced by adding 1 mM IPTG for 12 hours at 28°C with a shake speed of 220 rpm. The pellets were collected by centrifugation and stored at −80°C.

LDH purification

Five grams of cell pellets was suspended in 50 ml of tris-HCl solution [20 mM tris and 250 mM NaCl (pH 8.0)] with lysozyme (100 μg/ml). The cell suspensions were sonicated for 1 hour using an ultrasonicator (FB120220, Fisher Scientific). The supernatant was collected through centrifugation at 15,000*g* for 30 min and mixed with 5 ml of Ni–nitrilotriacetic acid (Ni-NTA) beads (GenScript). The beads were washed with tris-HCl solution two times after incubation at 4°C for 1 hour and then put into an affinity chromatography column (12 ml; Sangon Biotech). The impure proteins were removed using 6 ml of wash buffer (20 mM imidazole in tris-HCl solution) three times. The LDH proteins were collected by 10 ml of elution buffer (300 mM imidazole in tris-HCl solution). The LDH samples were kept at 4°C ready for subsequent photocatalytic TMP reduction.

FDH expression and purification

Seed cultures ($Tc_{Receiver}$/$CsgA_{A7}$-FDH) were inoculated from frozen glycerol stocks and grown in LB medium with chloramphenicol antibiotics (34 μg/ml). Cells were centrifuged and resuspended in the same volume of glucose supplementary M63 culture medium. The resuspended cells were used as seeds and added to glucose supplementary M63 culture medium with 10 μM K_2WO_4 at a volume ratio of 1:100. The strains were grown for 3 days at 30°C without shaking for FDH expression induced by the constitutive promoter J23108. The pellets were collected and resuspended in tris-HCl buffer. The cells were completely broken using a high-pressure homogenizer (JNBIO) at 1500 MPa. The supernatant was collected through centrifugation (Beckman Coulter) at 20,000*g* for 40 min and incubated with Ni-NTA beads (GenScript) at 4°C overnight. The impure proteins were removed using wash buffer (20 mM imidazole). The target proteins were collected through gradient elution with 100, 200, and 500 mM imidazole. The collected samples were kept at 4°C for SDS-PAGE and Western blot experiments.

SDS-PAGE

Fifteen microliters of purified protein solution was mixed with 5 μl of 4× loading buffer (Life Technologies). The mixed solution was boiled for 10 min for protein denaturation. The processed solution was added to the lane of 12% polyacrylamide gel (GenScript), which was put into tris-Mops-SDS running buffer (GenScript) with an applied 120-V voltage for 60 min and then stained using 0.25% Coomassie Brilliant blue. The SDS image was obtained by the ChemiDoc MP system (Bio-Rad).

Western blot

The proteins in polyacrylamide gel were blotted on nitrocellulose membrane using iBlot 2 Gel Transfer Device (Life Technologies). The nitrocellulose was blocked with 5% nonfat dry milk (Solarbio) in Tween 20 supplemented with tris (TBST) buffer for 30 min and washed with TBST buffer two times. The membrane was incubated in primary anti-His antibody (TransGen Biotech) for 2 hours and washed with TBST buffer two times, followed by incubation with second anti–horseradish peroxidase antibody (TransGen Biotech) for 1 hour and washed with TBST buffer three times. The resultant membrane was incubated with Clarity Western ECL Substrate (Bio-Rad) solution in a dark environment at room temperature for 1 min and imaged through the ChemiDoc MP system (Bio-Rad).

Transient photocurrent test

The photocatalyst-mineralized biofilms or unmineralized $CsgA_{A7}$ biofilms were collected through centrifugation from 20 ml of culture medium (after 2 days cultivation) and resuspended in 200 μl of ddH_2O. The solution was dropped onto FTO-conductive glass (10 mm by 10 mm). Then, FTO was put into the incubator at 37°C overnight and served as the working electrode. A three-electrode system was adopted for the measurement of transient photocurrent. The platinum wire was used as the counter electrode, while the Ag/AgCl was used as the reference electrode. Na_2SO_4 (0.5 M) was used as the electrolyte solution. The solution was purged by N_2 flow for 30 min. The measurements were conducted at room temperature with a constant N_2 flow under the illumination of a Xe lamp (CEL-HXF300) with the intensity of 0.31 W (PL-MW2000 Photoradiometer, Perfect Light). The data were collected using an electrochemical station (Chi 660E).

Synthesis procedure for $[Cp^*Rh(bpy)H_2O]^{2+}$

$[Rh(Cp^*)Cl_2]_2$ (7.7 mg) was dissolved in 4 ml of methanol in a vial with the orange color. 2,2′-Bipyridyl (3.9 mg) was added to the vial to make a yellow solution. Ten milliliters of diethyl ether was added to the solution. Then, the mixed solution was evaporated through a rotary evaporator (PC 3001 VARIO, VACUUBRAND) to form the compound $[Cp^*Rh(bpy)Cl]^{2+}$. A 2.5 mM $[Cp^*Rh(bpy)H_2O]^{2+}$ solution was obtained through the addition of 5 ml of ddH_2O, and the solution was kept in the 4°C refrigerator under dark condition.

Photocatalytic reduction of NAD^+

NAD^+ reduction

The 1-ml reaction system contained 1.5% TEOA, 1 mM NAD^+, 0.25 mM $[Cp^*Rh(bpy)H_2O]^{2+}$, and the photocatalyst-mineralized biofilms (the pellets were collected from 20 ml of M63 culture medium) in tris-HCl solution (pH 8.0). The reaction was performed under the illumination of artificial light-emitting diode (LED) (455 to 460 nm) arrays with the intensity of 0.013 W (PL-MW2000 Photoradiometer, Perfect Light). The absorption at 340 nm for the supernatant was monitored with a 0.5-hour interval using a microplate reader (Cytation 5, BioTek).

Repeated reduction of NAD^+

In this experiment, the 1-ml reaction solution was composed of 1 mM NAD^+, 1.5% TEOA, 0.25 mM $[Cp^*Rh(bpy)H_2O]^{2+}$, and the photocatalyst-mineralized biofilms (the pellets were collected from 20 ml of M63 culture medium) in tris-HCl solution (pH 8.0). The absorption of the supernatant at 340 nm after centrifugation was recorded after 3 hours under the illumination of artificial LED (455 to 460 nm) arrays with the intensity of 0.013 W (PL-MW2000 Photoradiometer, Perfect Light). The absorption at 340 nm for the supernatant was monitored using a microplate reader (Cytation 5, BioTek). Then, the precipitate was redispersed in the reaction solution. The reaction proceeded for another 3 hours until the end. The same experiments were repeated four times to assess the recyclability of the system. The absorption value of each cycle is divided by the first one as the relative activity. The instrument setup was shown in fig. S18.

Photocatalytic reduction of TMP into L-tert-leucine

The reaction system was 1 ml of tris-HCl solution containing LDH (1, 2, or 3 mg/ml), 1.5% TEOA, NAD^+ (1, 5, or 10 mM), 0.25 mM $[Cp^*Rh(bpy)H_2O]^{2+}$, 10 mM TMP, 10 mM NH_4Cl, and the photocatalyst-mineralized biofilms (the pellets were collected from 20 ml of M63 culture medium). The reaction vials were placed in the 1-liter beaker supplemented with 800 ml of ddH_2O, and the reaction was performed for 48 hours under the illumination of artificial LED (455 to 460 nm) arrays with the intensity of 0.013 W (PL-MW2000 Photoradiometer, Perfect Light). The supernatant after centrifugation was collected for NMR experiment to determine the concentrations of L-tert-leucine. The instrument setup was shown in fig. S18.

Photocatalytic reduction of MV^{2+}

The reaction system contained 1 mM MV^{2+}, 1.5% TEOA, and the photocatalyst-mineralized biofilms (the pellets were collected from 20 ml of M63 culture medium) in 3 ml of tris-HCl solution. The cuvette was put into a hood under the white light illumination with the intensity of 52 μW (Model 1918-R, Newport). The UV-vis spectra were recorded after 12 hours of illumination.

Synthesis of carboxyl-capped CdS NPs

We synthesized carboxyl-capped CdS NPs following a modified protocol based on a previous literature (*40*). Briefly, 3.87 μl of 3-mercaptopropionic acid was dissolved in 100 ml of deionized water, followed by slow addition of 100 μl of 2 M $Cd(NO_3)_2$ solution with continuous stirring (300 rpm) at room temperature. Then, the pH was adjusted to 9 with ammonium hydroxide (NH_4OH). Next, a clear yellowish suspension of CdS NPs was obtained by quick addition of 150 μl of 2 M Na_2S solution with constant stirring (300 rpm). Last, the solution was concentrated to 20 ml by rotary evaporator at 40°C.

Photocatalytic reduction of CO_2

The 5-ml reaction solution containing 5 mM MV, 10 mM ascorbic acid, 100 mM $NaHCO_3$, and the photocatalyst-mineralized biofilms (the pellets were collected from 20 ml of M63 culture medium or 0.2 mM synthesized CdS NPs and $Tc_{Receiver}/CsgA_{A7}$-FDH cells expressing only FDH enzymes) in PBS solution (pH 7.4) was added to a vial, which was illuminated under the xenon lamp (CEL-HXF300, CEAULIGHT) with a 420-nm optical filter for 8 hours. The intensity of the lamp was measured to be 0.12 W (PL-MW2000 Photoradiometer, Perfect Light). The distance from the reaction vial to light source was set at 26 cm. The supernatant after centrifugation was collected for NMR test to determine the concentrations of formic acid. The instrument setup was shown in fig. S27.

CR binding and CV staining assay

$Tc_{Receiver}/CsgA_{A7}$ seed cells were added to 20 ml of glucose-supplemented M63 culture medium and then cultivated for 72 hours at 30°C without shaking. Then, the biofilms were collected through centrifugation.

CR binding

The collected biofilms were resuspended in 1-ml PBS solution (pH 7.4). Ten microliters of CR solution (25 mg/ml) was added to the biofilm solution (1 ml). Then, the mixed solution was incubated for 10 min at room temperature. After centrifugation, the absorbance of the supernatant at 495 nm designated as A_t was measured using Cytation (BioTek), while the absorbance of CR (25 mg/ml) designated as A_0 was also measured. The CR binding to biofilms was calculated through subtraction of A_t from A_0.

CV staining

The collected biofilms were resuspended in 4-ml PBS solution (pH 7.2). Thirty microliters of CV solution (0.1%) was added to the biofilm solution (1 ml). Then, the mixed solution was incubated for 10 min at room temperature. After centrifugation, the absorbance of the supernatant at 550 nm designated as A_t was measured using Cytation (BioTek), while the absorbance of 0.1% CR designated as A_0 was also measured. The CV staining to biofilms was calculated through subtraction of A_t from A_0.

The control experiments were performed without Tc in the culture medium. Each test was repeated four times. The data were presented in fig. S3.

Live/dead staining

The bacterial samples were collected through centrifugation and resuspended in 0.85% NaCl solution at a final optical density at 600 nm of 1. The dye mixtures containing 1.5 μl of SYTO9 and 1.5 μl of propidium iodide (LIVE/DEAD BacLight Bacterial Viability Kits, Thermo Fisher Scientific) were added to 1 ml of bacterial suspension. Then, the solution was mixed and incubated at dark condition for 15 min. Last, 5 μl of the stained samples was dropped and trapped between a slide and a 18-mm square coverslip. The fluorescence images were observed using Olympus FV3000.

Transmission electron microscopy

The sample solution was dropped on the TEM grid (Zhongjingkeyi Technology) directly, which was incubated at ambient environment for 5 min. The excessive sample solution was wicked away with filter paper, and the grid was rinsed with ddH_2O two times by dropping on TEM grid and quickly wicking off with filter paper. The sample was negatively stained with 10 μl of uranyl acetate (2 weight %)

for 1 min. The excessive uranyl acetate was wicked off, and the sample was desiccated for 20 min under an infrared lamp (Zhongjingkeyi Technology). TEM images were obtained on a FEI T12 TEM operated at 120-kV accelerating voltage. HRTEM, SAED, HAADF-STEM, and EDS mapping were performed on a JEM-F200 operating at 200-kV accelerating voltage or a JEM-ARM300F(w_d) electron microscope operating at 300-kV accelerating voltage.

UV-vis spectra

The biofilm samples were collected and washed with ddH_2O two times then dried through freeze-drying using a vacuum freeze dryer (Labconco FreeZone 2.5). Then, the samples were grinded with $BaSO_4$ powder using a mortar under the infrared lamp. UV-vis DRS were recorded using a UV-vis-NIR (near-infrared) spectrometer (Agilent Cary 5000) with samples in integrating sphere. For samples in the solution, the UV-vis spectra were directly recorded using a UV-vis-NIR spectrometer (Agilent Cary 5000).

Nuclear magnetic resonance

NMR was carried out to measure the production of L-tert-leucine and formic acid. The test solution was a 0.5-ml PBS solution containing 50 μl of D_2O, 50 μl of DSS (5 mM) as internal standard, 50 μl of sample solution, and 350 μl of PBS solution. The NMR data were recorded using AVANCE NEO 400 or AVANCE III HD50 (Bruker). The collected data were processed and integrated using Bruker TopSpin software.

Inductively coupled plasma optical emission spectrometer

To monitor the free Cd^{2+} ion concentration during the preparation process of the photocatalyst-mineralized biofilms, the supernatant after centrifugation collected at different time intervals was preserved in a 4°C refrigerator for subsequent measurement. ICP-OES measurements were performed using ICP-OES iCAP 7400 (Thermo Fisher Scientific). The collected data were processed using the Origin software. The experiments were repeated at least three times.

X-ray photoelectron spectroscopy

The freeze-dried samples were pressed into thin pieces by the tablet machine for subsequent measurement. The pressed samples were placed in the sample stage and transferred to the vacuum chamber of ESCALAB 250Xi (Thermo Fisher Scientific). Then, the data were collected using a spot size of 400 μm with charge compensation. The data were exported using the Avantage software and processed using the Origin software. The spectra were calibrated by 284.8 eV of C1s.

LC-MS spectra

LC-MS experiment was carried out in positive ion mode with a quadrupole time-of-flight mass spectrometer (Agilent QTOF 6550) equipped with a high-performance LC (Agilent 1260). Last, deconvolution was performed with Agilent MassHunter Qualitative Analysis B.06.00 software with BioConfirm workflow. The plot was redrew using the Origin software.

SUPPLEMENTARY MATERIALS

Supplementary material for this article is available at https://science.org/doi/10.1126/sciadv.abm7665

View/request a protocol for this paper from *Bio-protocol*.

REFERENCES AND NOTES

1. A. Y. Chen, C. Zhong, T. K. Lu, Engineering living functional materials. *ACS Synth. Biol.* **4**, 8–11 (2015).
2. P. Q. Nguyen, N. D. Courchesne, A. Duraj-Thatte, P. Praveschotinunt, N. S. Joshi, Engineered living materials: Prospects and challenges for using biological systems to direct the assembly of smart materials. *Adv. Mater.* **30**, e1704847 (2018).
3. C. Gilbert, T. Ellis, Biological engineered living materials: Growing functional materials with genetically programmable properties. *ACS Synth. Biol.* **8**, 1–15 (2019).
4. T. C. Tang, B. L. An, Y. Y. Huang, S. Vasikaran, Y. Y. Wang, X. Y. Jiang, T. K. Lu, C. Zhong, Materials design by synthetic biology. *Nat. Rev. Mater.* **6**, 332–350 (2021).
5. X. B. Li, C. H. Tung, L. Z. Wu, Semiconducting quantum dots for artificial photosynthesis. *Nat. Rev. Chem.* **2**, 160–173 (2018).
6. S. S. Chen, T. Takata, K. Domen, Particulate photocatalysts for overall water splitting. *Nat. Rev. Mater.* **2**, 17050 (2017).
7. L. Cheng, Q. Xiang, Y. Liao, H. Zhang, CdS-based photocatalysts. *Energ. Environ. Sci.* **11**, 1362–1391 (2018).
8. J. Liu, Y. Zheng, Z. Hong, K. Cai, F. Zhao, H. Han, Microbial synthesis of highly dispersed PdAu alloy for enhanced electrocatalysis. *Sci. Adv.* **2**, e1600858 (2016).
9. Y. Cao, Y. Feng, M. D. Ryser, K. Zhu, G. Herschlag, C. Cao, K. Marusak, S. Zauscher, L. You, Programmable assembly of pressure sensors using pattern-forming bacteria. *Nat. Biotechnol.* **35**, 1087–1093 (2017).
10. D. H. Park, J. Cho, O. J. Kwon, C. O. Yun, J. H. Choy, Biodegradable inorganic nanovector: Passive versus active tumor targeting in siRNA transportation. *Angew. Chem. Int. Ed.* **55**, 4582–4586 (2016).
11. K. D. Wegner, Z. Jin, S. Linden, T. L. Jennings, N. Hildebrandt, Quantum-dot-based Förster resonance energy transfer immunoassay for sensitive clinical diagnostics of low-volume serum samples. *ACS Nano* **7**, 7411–7419 (2013).
12. Y. Shen, L. Posavec, S. Bolisetty, F. M. Hilty, G. Nystrom, J. Kohlbrecher, M. Hilbe, A. Rossi, J. Baumgartner, M. B. Zimmermann, R. Mezzenga, Amyloid fibril systems reduce, stabilize and deliver bioavailable nanosized iron. *Nat. Nanotechnol.* **12**, 642–647 (2017).
13. S. Cestellos-Blanco, H. Zhang, J. M. Kim, Y.-x. Shen, P. Yang, Photosynthetic semiconductor biohybrids for solar-driven biocatalysis. *Nat. Catal.* **3**, 245–255 (2020).
14. N. Kornienko, J. Z. Zhang, K. K. Sakimoto, P. Yang, E. Reisner, Interfacing nature's catalytic machinery with synthetic materials for semi-artificial photosynthesis. *Nat. Nanotechnol.* **13**, 890–899 (2018).
15. W. Wei, P. Sun, Z. Li, K. Song, W. Su, B. Wang, Y. Liu, J. Zhao, A surface-display biohybrid approach to light-driven hydrogen production in air. *Sci. Adv.* **4**, eaap9253 (2018).
16. C. Liu, B. C. Colon, M. Ziesack, P. A. Silver, D. G. Nocera, Water splitting-biosynthetic system with CO_2 reduction efficiencies exceeding photosynthesis. *Science* **352**, 1210–1213 (2016).
17. J. Guo, M. Suastegui, K. K. Sakimoto, V. M. Moody, G. Xiao, D. G. Nocera, N. S. Joshi, Light-driven fine chemical production in yeast biohybrids. *Science* **362**, 813–816 (2018).
18. K. K. Sakimoto, A. B. Wong, P. Yang, Self-photosensitization of nonphotosynthetic bacteria for solar-to-chemical production. *Science* **351**, 74–77 (2016).
19. Y. Ding, J. R. Bertram, C. Eckert, R. R. Bommareddy, R. Patel, A. Conradie, S. Bryan, P. Nagpal, Nanorg microbial factories: Light-driven renewable biochemical synthesis using quantum dot-bacteria nanobiohybrids. *J. Am. Chem. Soc.* **141**, 10272–10282 (2019).
20. D. P. Linklater, V. A. Baulin, X. Le Guevel, J. B. Fleury, E. Hanssen, T. H. P. Nguyen, S. Juodkazis, G. Bryant, R. J. Crawford, P. Stoodley, E. P. Ivanova, Antibacterial action of nanoparticles by lethal stretching of bacterial cell membranes. *Adv. Mater.* **32**, e2005679 (2020).
21. K. K. Sakimoto, N. Kornienko, S. Cestellos-Blanco, J. Lim, C. Liu, P. Yang, Physical biology of the materials-microorganism interface. *J. Am. Chem. Soc.* **140**, 1978–1985 (2018).
22. G. Liu, F. Gao, C. Gao, Y. Xiong, Bioinspiration toward efficient photosynthetic systems: From biohybrids to biomimetics. *Chem. Catalysis* **1**, 1367–1377 (2021).
23. L. Vidakovic, P. K. Singh, R. Hartmann, C. D. Nadell, K. Drescher, Dynamic biofilm architecture confers individual and collective mechanisms of viral protection. *Nat. Microbiol.* **3**, 26–31 (2018).
24. B. Halan, K. Buehler, A. Schmid, Biofilms as living catalysts in continuous chemical syntheses. *Trends Biotechnol.* **30**, 453–465 (2012).
25. R. L. DiMarco, S. C. Heilshorn, Multifunctional materials through modular protein engineering. *Adv. Mater.* **24**, 3923–3940 (2012).
26. S. H. Lee, D. S. Choi, S. K. Kuk, C. B. Park, Photobiocatalysis: Activating redox enzymes by direct or indirect transfer of photoinduced electrons. *Angew. Chem. Int. Ed.* **57**, 7958–7985 (2018).
27. K. E. Marusak, Y. Feng, C. F. Eben, S. T. Payne, Y. Cao, L. You, S. Zauscher, Cadmium sulphide quantum dots with tunable electronic properties by bacterial precipitation. *RSC Adv.* **6**, 76158–76166 (2016).
28. J. Kim, S. H. Lee, F. Tieves, D. S. Choi, F. Hollmann, C. E. Paul, C. B. Park, Biocatalytic C=C bond reduction through carbon nanodot-sensitized regeneration of NADH analogues. *Angew. Chem. Int. Ed.* **57**, 13825–13828 (2018).

29. X. Wang, J. Pu, Y. Liu, F. Ba, M. Cui, K. Li, Y. Xie, Y. Nie, Q. Mi, T. Li, L. Liu, M. Zhu, C. Zhong, Immobilization of functional nano-objects in living engineered bacterial biofilms for catalytic applications. *Natl. Sci. Rev.* **6**, 929–943 (2019).
30. F. Moser, E. Tham, L. M. Gonzalez, T. K. Lu, C. A. Voigt, Light-controlled, high-resolution patterning of living engineered bacteria onto textiles, ceramics, and plastic. *Adv. Funct. Mater.* **29**, 1901788 (2019).
31. A. Alissandratos, H. K. Kim, H. Matthews, J. E. Hennessy, A. Philbrook, C. J. Easton, *Clostridium carboxidivorans* strain P7T recombinant formate dehydrogenase catalyzes reduction of CO_2 to formate. *Appl. Environ. Microbiol.* **79**, 741–744 (2013).
32. Q. Wang, J. Warnan, S. Rodriguez-Jimenez, J. J. Leung, S. Kalathil, V. Andrei, K. Domen, E. Reisner, Molecularly engineered photocatalyst sheet for scalable solar formate production from carbon dioxide and water. *Nat. Energy* **5**, 703–710 (2020).
33. J. Barber, P. D. Tran, From natural to artificial photosynthesis. *J. R. Soc. Interface* **10**, 20120984 (2013).
34. Y. Su, S. Cestellos-Blanco, J. M. Kim, Y.-x. Shen, Q. Kong, D. Lu, C. Liu, H. Zhang, Y. Cao, P. Yang, Close-packed nanowire-bacteria hybrids for efficient solar-driven CO_2 fixation. *Joule* **4**, 800–811 (2020).
35. Y. Choi, S. Y. Lee, Biosynthesis of inorganic nanomaterials using microbial cells and bacteriophages. *Nat. Rev. Chem.* **4**, 638–656 (2020).
36. W. Qin, C.-y. Wang, Y.-x. Ma, M.-j. Shen, J. Li, K. Jiao, F. R. Tay, L.-n. Niu, Microbe-mediated extracellular and intracellular mineralization: Environmental, industrial, and biotechnological applications. *Adv. Mater.* **32**, e1907833 (2020).
37. J. Huang, S. Liu, C. Zhang, X. Wang, J. Pu, F. Ba, S. Xue, H. Ye, T. Zhao, K. Li, Y. Wang, J. Zhang, L. Wang, C. Fan, T. K. Lu, C. Zhong, Programmable and printable *Bacillus subtilis* biofilms as engineered living materials. *Nat. Chem. Biol.* **15**, 34–41 (2019).
38. Y. Zhou, D. Smith, B. J. Leong, K. Brannstrom, F. Almqvist, M. R. Chapman, Promiscuous cross-seeding between bacterial amyloids promotes interspecies biofilms. *J. Biol. Chem.* **287**, 35092–35103 (2012).
39. B. An, Y. Wang, X. Jiang, C. Ma, M. Mimee, F. Moser, K. Li, X. Wang, T.-C. Tang, Y. Huang, Y. Liu, T. K. Lu, C. Zhong, Programming living glue systems to perform autonomous mechanical repairs. *Matter* **3**, 2080–2092 (2020).
40. H. Li, W. Y. Shih, W. H. Shih, Synthesis and characterization of aqueous carboxyl-capped CdS quantum dots for bioapplications. *Ind. Eng. Chem. Res.* **46**, 2013–2019 (2007).

Acknowledgments: We thank the Analytical Instrumentation Center (AIC) and the Electron Microscopy Center (EMC) at School of Physical Science and Technology, ShanghaiTech University; the Shanghai Institute of Microsystem and Information Technology (SIMIT), and the National Center for Protein Science Shanghai. **Funding:** This work was partially funded by the National Key R&D Program of China (grant nos. 2020YFA0908100 and 2021YFA0910800), the National Science Fund for Distinguished Young Scholars (grant no. 32125023), and the China Postdoctoral Science Foundation (grant nos. 2019TQ0340 and 2019M661665). **Author contributions:** C.Z. directed the project. C.Z., X.W., and J.Z. conceived the technical details and designed the experiments. K.L. performed the photocatalytic experiment. B.A. performed the plasmid construction for pZA-CmR-rr12-pL(tetO)-CG-*csgA*$_{A7}$. Y.W. carried out the experiments in the "Inductively coupled plasma optical emission spectrometer" section. C.Z., X.W., and J.Z. analyzed the data, discussed the results, and wrote the manuscript with help from all the authors. All the authors revised the manuscript. **Competing interests:** The authors declare that they have no competing interests. **Data and materials availability:** All data needed to evaluate the conclusions in the paper are present in the paper and/or the Supplementary Materials.

Submitted 11 October 2021
Accepted 22 March 2022
Published 6 May 2022
10.1126/sciadv.abm7665